www.MaterialsViews.com

Large-Scale Horizontally Aligned ZnO Microrod Arrays with Controlled Orientation, Periodic Distribution as Building Blocks for Chip-in Piezo-Phototronic LEDs

Zhen Guo, Haiwen Li, Lianqun Zhou, Dongxu Zhao, Yihui Wu, Zhiqiang Zhang, Wei Zhang, Chuanyu Li, and Jia Yao*

***A** novel method of fabricating large-scale horizontally aligned ZnO microrod arrays with controlled orientation and periodic distribution via combing technology is introduced. Horizontally aligned ZnO microrod arrays with uniform orientation and periodic distribution can be realized based on the conventional bottom-up method prepared vertically aligned ZnO microrod matrix via the combing method. When the combing parameters are changed, the orientation of horizontally aligned ZnO microrod arrays can be adjusted (θ = 90° or 45°) in a plane and a misalignment angle of the microrods (0.3° to 2.3°) with low-growth density can be obtained. To explore the potential applications based on the vertically and horizontally aligned ZnO microrods on p-GaN layer, piezo-phototronic devices such as heterojunction LEDs are built. Electroluminescence (EL) emission patterns can be adjusted for the vertically and horizontally aligned ZnO microrods/p-GaN heterojunction LEDs by applying forward bias. Moreover, the emission color from UV-blue to yellow-green can be tuned by investigating the piezoelectric properties of the materials. The EL emission mechanisms of the LEDs are discussed in terms of band diagrams of the heterojunctions and carrier recombination processes.*

1. Introduction

The large-scale fabrication of horizontally aligned micro- and nanostructure with a specific alignment orientation on a wafer is critically important in the integration of chip in laboratory devices. A single micro- or nanostructure can be manipulated using optical tweezers. However, large-scale manipulation is time consuming. Given the developments

Z. Guo, H. Li, L. Zhou, Z. Zhang, W. Zhang, C. Li, J. Yao
Key Lab of Bio-Medical Diagnostics
Suzhou Institute of Biomedical
Engineering and Technology
Chinese Academy of Sciences
No.88-Keling Road, Suzhou New District
215163, PR China
E-mail: happygzh2000@163.com

Prof. D. Zhao
The State Key Laboratory of Luminescence and Applications
Changchun Institute of Optics
Fine Mechanics and Physics
Chinese Academy of Sciences
3888 East Nan-Hu Road
Open Economic Zone
Changchun 130033, PR China

Prof. Y. Wu
The State Key Laboratory of Applied Optics
Changchun Institute of Optics
Fine Mechanics and Physics
Chinese Academy of Sciences
3888 East Nan-Hu Road
Open Economic Zone
Changchun 130033, PR China

DOI: 10.1002/smll.201402151

small NANO MICRO

in micro- and nanotechnology, the large-scale manipulation of micro- or nanostructure is one of the most challenging yet promising in micro- or nanodevice applications. Given that ZnO, an excellent member of the family of one-dimensional micro- or nanostructures, is a direct wide-bandgap (3.3 eV) semiconductor with an exciton binding energy of 60 meV, it can be applied in laser-emitting units,[1–4] field-emitting transistors,[5–7] photon detectors,[8–10] and generators.[11–14] As such, ZnO micro- or nanostructures can be utilized as highly efficient and stable exciton ultraviolet (UV) emission materials at room temperature.[1,15] In addition, ZnO is a well-known piezoelectric material that has potential applications in microelectromechanical systems as nanoforce sensors and nanogenerators, and in communications as surface acoustic wave.[16–18] When the bottom-up or top-down methods are used, carbon nanotubes,[19,20] silicon nanowires (NWs),[21–23] boron NWs,[24] and InGaAs nanopillar[25,26] can be prepared from plane nanomaterials. Up to date, few studies have reported the preparation of horizontally aligned micro- or nanostructure arrays via a confined growth procedure[27,28] or feeding gas flow.[29] However, no study has been reported on the fabrication of large-scale horizontally aligned microstructure arrays with designed orientation and periodic distribution on *p*-type GaN to realize the potential functions of the microstructures as piezo-phototronic light emitting diode (LED) devices in a plane. In the current study, a new method was developed to obtain large-scale horizontally aligned ZnO microrod arrays with periodic alignment on *p*-GaN layer via the combing technology. To couple the piezoelectric and wide-bandgap semiconductor properties in ZnO, LEDs that are based on vertically and horizontally aligned ZnO microrods/*p*-GaN heterojunction were fabricated. Spot and line-shaped EL emission images demonstrated the different alignments of the ZnO microrods on *p*-GaN, as well as the different radiative recombination mechanisms of the emitted photons with different wavelengths at forward bias. To obtain horizontally aligned ZnO microrods with specific patterns, two steps were considered. First, vertically aligned ZnO microrods were selectively prepared on the exposed *p*-GaN template via hydrothermal method. Second, large-scale horizontally aligned ZnO microrod arrays with periodic alignment were obtained via combing technology. The orientation of the horizontally aligned ZnO microrod arrays can be adjusted with $\theta = 45°$ or 90° on a plane.

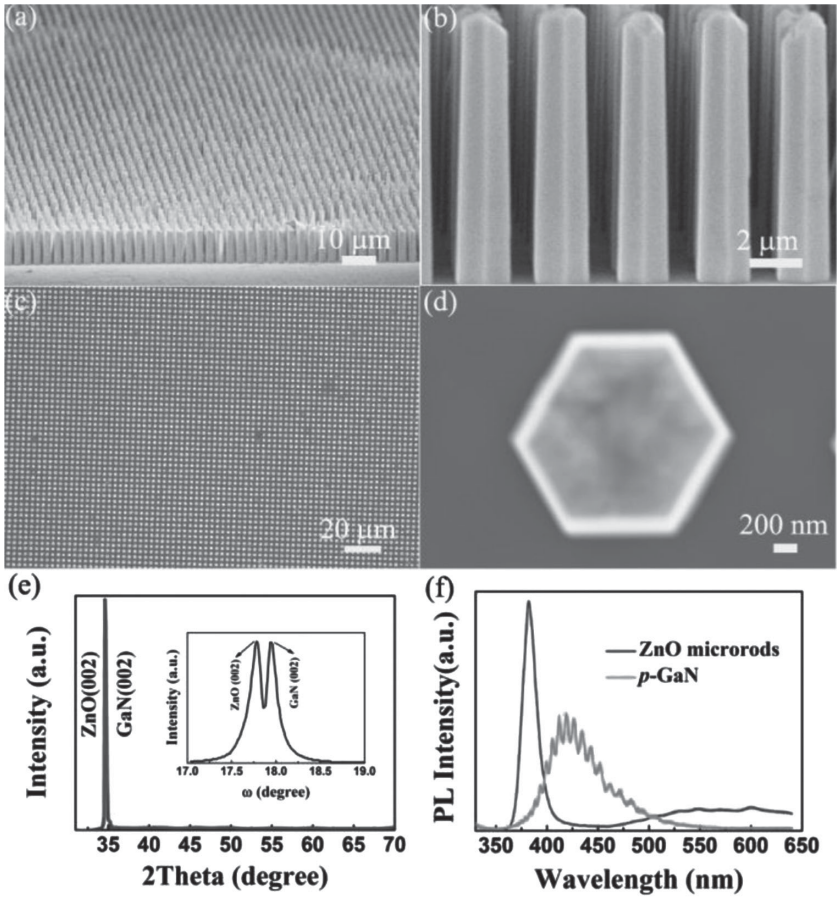

Figure 1. (a,b) the cross-sectional SEM images with different magnification of the vertically aligned ZnO microrod arrays grown on the exposed *p*-GaN template direct written with EBL method. (c) Large scale top view SEM image of the vertically aligned ZnO microrods. (d) the top of single ZnO microrod showed well faceted hexagonal morphology. (e) Wide-range XRD 2θ-scan of the vertically aligned ZnO microrod arrays grown on *p*-GaN/sapphire substrate, the inset shows X-ray diffraction (XRD) ω-scan curve. (f) the PL spectra of ZnO microrods and *p*-GaN wafer.

2. Results and Discussion

As shown in the scanning electron microscopy (SEM) images in **Figure 1**(a, c), large-scale (up to 40 000 μm^2) ZnO microrod arrays that were selectively grown on electron beam lithography (EBL)-exposed *p*-GaN layer with few imperfection points can be obtained via the hydrothermal method. Excellent vertically aligned ZnO microrod (interspace: 3 μm) arrays were obtained (Figure 1b). The atomic ratio of O to Zn is 51:49 for the epitaxial ZnO analyzed by energy spectrum attached to FESEM indicates almost equal amount of the elements for forming the microrod. The top-view SEM image of the vertically aligned ZnO microrod arrays (Figure 1c) illustrated good homogeneity with only 1‰ bad points. The magnified SEM image of a single hexagonal ZnO microrod with a diameter of 2 μm (which is in accordance with the size of the exposed PMMA) was obtained (Figure 1d). As shown in Figure S1, relatively homogenoeus vertically aligned ZnO microrods with diameter of 2 μm were

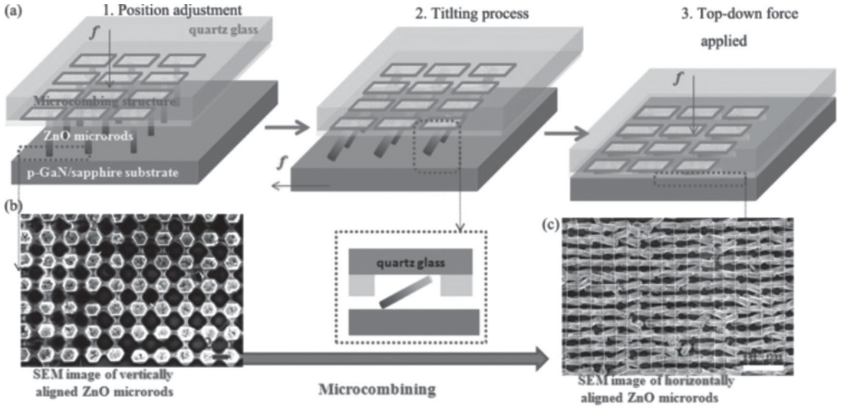

Figure 2. Schematic illustration of preparing horizontally aligned ZnO microrod arrays. (a) schematics of the combing process, the red arrow indicates the direction of the force applied on the combing structure/quartz glass or *p*-GaN/sapphire substrate, which yields a combing force combined with the restricted region for the ZnO microrods horizontally aligned on *p*-GaN layer, the dashed window in the middle shows a side view during combing process. (b) SEM image of the vertically aligned ZnO microrod arrays spin coated with PMMA resist. (c) Top view SEM image of the horizontally aligned ZnO microrod arrays after combing process.

obtained in a large scale on commercially obtained *p*-GaN compared with others (diameters: 500 nm, 200 nm, and 1 μm). As shown in Figure S2, the vertically aligned ZnO microrods with diameter of up to 20 μm could be obtained via hydrothermal method using photoresist as a mask, the magnified SEM image of the ZnO microrod shows quasi-hexagnol morphology. As shown in Figure S3 the ZnO microrod line arrays composed of low density or closely packed distribution patterns were observed by changing the solution concentration. Figure 1e shows the wide range (30° to 70°) X-ray diffraction 2θ-scan of the vertically aligned ZnO microrod arrays that were grown on *p*-GaN template. Only one diffractive peak at 34.5° was observed, which corresponds to the (002) direction of the ZnO diffractive peak. This result indicates that the ZnO microrod arrays are in the *c*-axis preferred orientation. Given that the lattice parameters of ZnO and GaN are very close to one another, a ω-scan was performed to identify the diffractive peaks of ZnO (002) and GaN (002). The (002) diffractive peaks that originated from ZnO and GaN (insert of Figure 1e) could be clearly distinguished with the corresponding narrow full width at half maximum (FWHM) values of 0.16° and 0.12°, which revealed the good crystal quality of the vertically aligned ZnO microrods. Figure 1f shows the room temperature photoluminescence (PL) spectra of the selectively grown ZnO microrod arrays on the *p*-GaN wafer. The spectrum of the ZnO displayed a dominant sharp near-band-edge emission at 380 nm, which is accompanied by a weak defect-related emission band ranging from 475 nm to 700 nm. A broad PL emission band ranging from 365 nm to 570 nm with a dominant peak centered at approxiamtely 421 nm was observed for the *p*-GaN wafer, which is frequently observed in Mg-doped *p*-GaN. This band corresponds to the transitions between conduction-band electrons or donors and Mg-related acceptors. The observed fringes in the spectrum are caused by the interference between GaN/air and sapphire/GaN interfaces.

Figure 2a shows the schematics of preparing horizontally aligned ZnO microrod arrays on a *p*-GaN/sapphire substrate. First, the vertically aligned ZnO microrods on *p*-GaN/sapphire substrate were loaded in a wafer holder (Figure S4), and the combing structure on quartz glass (Figure S5) was loaded in a mask holder. The vertically aligned ZnO microrods can be confined in the designed combing-patterned structure by using positive alignment markers with the use of a microscope. When almost all of the top facets of the ZnO microrods were completely confined in the combing structure, they were inclined by changing the *x*-axis, *y*-axis, or θ-angle rotation on the plane (depending on the preferred direction of the horizontal alignment of the microrods) of the sample holder for only several micrometers or certain degrees. Finally, the *z*-axis position of the mask holder was adjusted to ensure that all ZnO microrods are horizontally aligned to the combing structure. Figure 2b shows the top-view SEM image of the vertically aligned ZnO microrod arrays that were spin-coated with the PMMA resist. The PMMA that adhered to the vertically aligned ZnO microrod matrix structure was used to locate the microrods during the combing process (Figure S6). When the combing technique was used, horizontally aligned microrods was obtained after intentionally applying a position shift on the sample holder (Figure 2c). The horizontally aligned microrods displayed linear alignment morphology by only one direction shift of the axis during the combing procedure, and the top parts of the microrods are closely packed with the roots of another. The domino effect is significant in forming the horizontal alignment of closely packed ZnO microrod arrays during the combing process. Several parallel lines could be intentionally drawn based on the orientation of the horizontally aligned ZnO microrods. The average interspace of these lines was approximately 3 μm, which is consistent with the designed value for the vertically aligned microrods. Each microrod remained in its own position after the combing process. For comparison, the transformation procedure from the vertically to horizontally aligned ZnO microrods without PMMA coating were also performed. As shown in Figure S7, the horizontally placed ZnO microrods with disordered distribution morphology were obtained.

Figures 3a and S8 show the top-view SEM images of the large-scale (up to 10000 μm^2) horizontally aligned ZnO microrod arrays with excellent homogeneity that can be obtained via the combing technique; a linear alignment was observed for all microrods. The magnified SEM image of the horizontally aligned ZnO microrods shows periodic distribution after careful observation (Figure 3b). Several transverse and longitudinal parallel lines can be drawn based on the orientation and top positions of the horizontally aligned ZnO microrods (Figure 3c), from which periodic squares can be formed. As such, the horizontally aligned ZnO microrods exhibit good alignment in a large scale. The orientation of the horizontally aligned ZnO microrods can also be adjusted by changing the θ-angle in the plane of the sample holder during

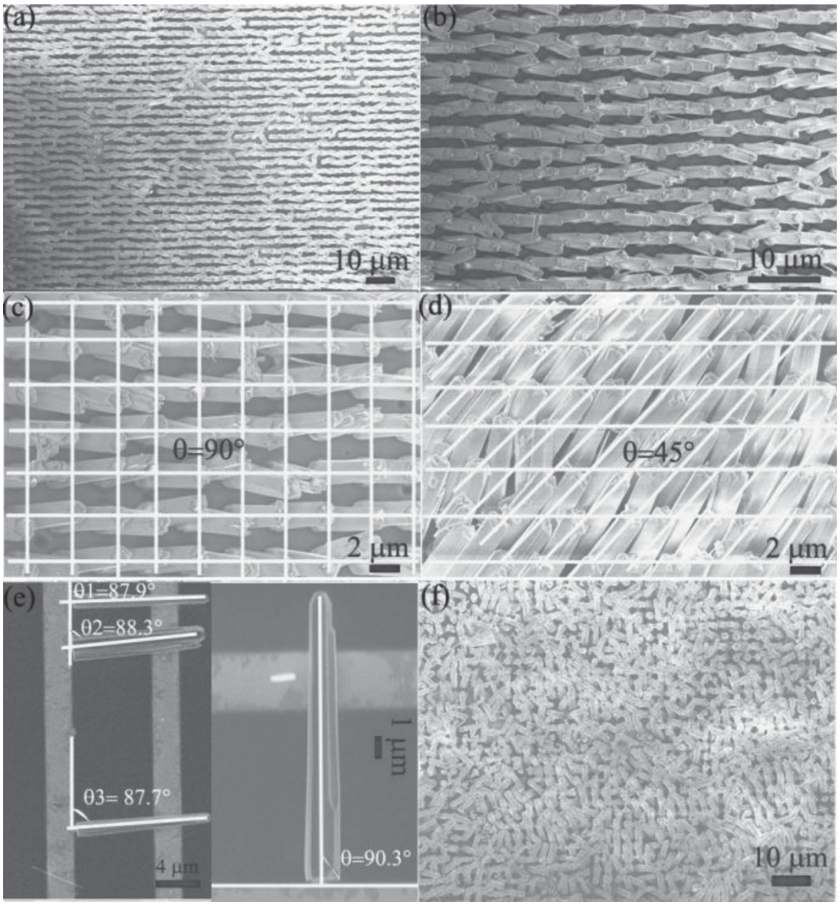

Figure 3. (a) SEM image of horizontally aligned ZnO microrod arrays with large scale up to 10000 μm^2, (b) magnified SEM image of horizontally aligned ZnO microrods with periodic distribution, (c,d) square, bevel shaped grids could be drawn based on the horizontally aligned ZnO microrods with $\theta = 90°$ and 45° respectively. (e) SEM image of horizontally aligned ZnO microrods with low density. (f) SEM images of horizontally random distributed ZnO microrods by applying top-down force.

the combing process (Figure 3d). Similarly, several bevel-shaped grids can be drawn, and the obtained angle for the bevel-shaped grids was approximately 45°, demonstrating the orientation adjustment of the horizontally aligned ZnO microrods. Figure 3e shows that horizontally aligned ZnO microrods with low density were also formed via the combing technology, and an angle shift (0.3° to 2.3°) of the microrod orientation from the targeted direction could be obtained. The transformation from the vertically to the horizontally aligned ZnO microrods with periodic, low density distribution could also be obtained with little imperfection using combing technology (Figures S9,10). For comparison, without using combing structure, the horizontally oriented and randomly distributed ZnO microrods were obtained when only top-down force was applied on the quartz glass during the combing procedure (Figure 3f).

As shown in the inserts of **Figure 4**(a, c), *p–n* heterojunction LEDs can be built based on the vertically and horizontally aligned ZnO microrods (the intrinsic carrier concentration for the ZnO with *n*-type can be larger than 10^{17} cm^{-3}, electron mobility of the unintentionally doped ZnO could be 13 ± 5 cm^2 V^{-1} S^{-1}) on *p*-GaN layer (the hole concentration and mobility were 3.0×10^{17} cm^{-3} and 10 cm^2 V^{-1} S^{-1}, respectively).[30,31] To fabricate a diode, the PMMA resist with a thickness of several micrometers was spin-coated on the aligned ZnO microrods and was used as the filling insulator layer. The top layer of the PMMA was then cleaned with oxygen plasma to form an ideal contact between the top electrode and the ZnO microrods. Ni/Au alloy and ITO conductive film with a low resistance were used as the electrodes for the *p*-GaN wafer and the aligned ZnO microrods, respectively. Compared with the *I–V* characteristics of the vertically aligned ZnO microrods/*p*-GaN heterojunction LED, a lower injection current with a larger threshold voltage of 7 V was observed for the horizontally aligned ZnO microrods/*P*-GaN LED, thereby indicating that a large carrier barrier was possibly built between the horizontally aligned microrods and the *p*-GaN layer, and the obtained injection current was in the order of 10 μA. In our experiment, the linear curve for Ni/Au on *p*-GaN revealed that good Ohmic contacts were formed in the electrodes (Figure S11). Low-resistance ITO conductive film can form good Ohmic contact with ZnO.[32] As shown in Figure S12, small energy band steps ΔE_C for an electron is $\Delta E_C = \chi_{(GaN)} - \chi_{(ZnO)} = (4.2 - 4.35) = -0.15$ eV, and the energy barrier ΔE_V for a hole is $\Delta E_V = E_{g(GaN)} + \Delta E_C - E_{g(ZnO)} = 3.39 - 0.15 - 3.37 = -0.13$ eV was formed under balance state. Therefore, the nonlinear behavior of the LEDs originated from the horizontally aligned ZnO microrod/*p*-GaN. No intentional carrier blocking barrier was inserted between ZnO and *p*-GaN. Thus, the interface between ZnO and GaN may cause a large voltage threshold for horizontally aligned ZnO microrods/*p*-GaN heterojunction. As displayed in **Figure 4**b, the EL spectrum of the vertically aligned ZnO microrods/*p*-GaN LED under forward bias can be divided into four individual peaks by the Gauss analysis; the main emission peak of the EL spectrum is comprised of a UV emission at 383 nm and a blue emission at 402 nm. The fitted EL emission bands located at 383, 402, and 432 nm could be attributed to the near-bandgap excitonic emission in ZnO microrods, the transitions from the conduction band edge of ZnO to the acceptor level of GaN, and the donor level E_D in ZnO to the acceptor level E_A in GaN. The weak EL emission at 585 nm could be attributed to the transition from the donor level E_D to the defects energy level E_d in ZnO, because defect-related emission always reflect a broad peak. As shown in the insert of Figure 4b, the UV–blue EL bright spot pattern of the vertically aligned ZnO microrods/*p*-GaN heterojunction LED could be observed with an optical microscope, through which the bright light emission with hexagnol morphology could be captured, which is in accordance with the

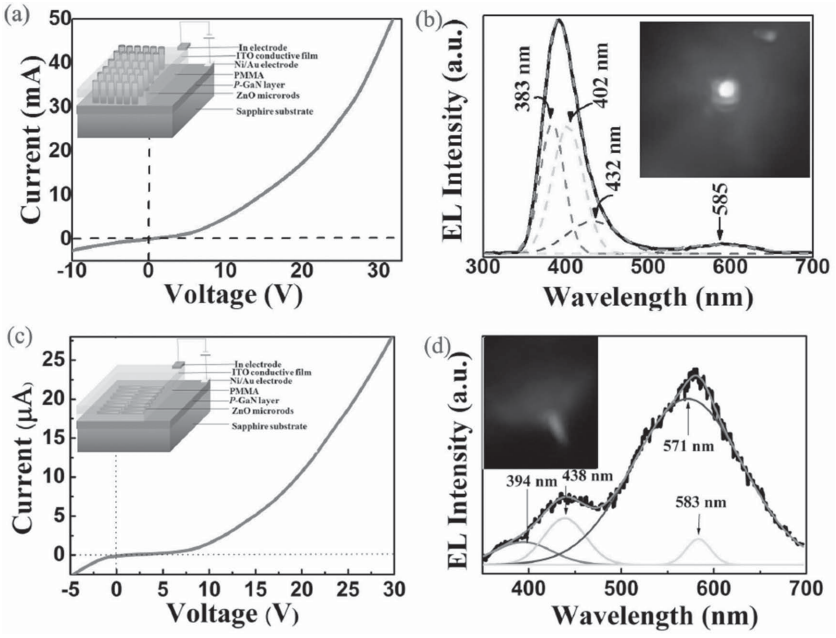

Figure 4. (a,c) I-V characteristics of the vertically and horizontally aligned ZnO microrods/*p*-GaN heterojunction LEDs, the inserts show the schematics of the fabricated LEDs, (b,d) EL spectra of the vertically and horizontally aligned ZnO microrods/*p*-GaN heterojunction LEDs (the black curves indicate the obtained EL spectra, and the color curves indicate the composition of the EL spectra, the inserts show the optical images of the LEDs at forward bias.

hexagnol morphology of ZnO microrod. In addition to the luminescence center, six side-scattering light lines with weak emission could also be recorded because of the hexagnol morphology of ZnO microrod. Figure S13 shows the optical EL image of each individual light emission spots in a large scale based on the vertically aligned ZnO microrods/*p*-GaN LED. Careful examination of this image led to the identification of one-dimensional ZnO material as a good waveguide material, inside a whispering gallery mode resonator wherein the lightwave could circulate because of multiple total internal reflection at the resonator boundaries.[33–35] Strong raddiative recombination occurred in the vertically aligned ZnO microrods/*p*-GaN heterojunction LED, and the discrete UV–blue emission spots could be clearly observed even in daily light (Figure S14). The patterned EL image of the vertically aligned ZnO microrods/*p*-GaN LED with UV–blue emission could also be obtained (Figure S15). However, strong broad yellow–green deep energy level-related emission bands located at 571 and 583 nm, accompanied with purple–blue emissions located at 394 and 438 nm (Figure 4d) were observed for the EL spectra of the horizontally aligned ZnO microrods/*p*-GaN LED. The EL spectrum of the vertically aligned ZnO microrod/*P*-GaN heterojunction LED shows that the strong emission band ranging from 500 nm to 700 nm could be ascribed to the defect-related emission in ZnO, which can be attributed to the increased interfacial recombination that were built between ZnO and *P*-GaN during combing procedure. The decreased UV–blue emission accompanied by redshifted EL emission at 394 nm could be ascribed to the near-bandgap exciton emission in ZnO microrods. The emission at 438 nm may have originated from the transition in the *p*-GaN layer. The optical image of the horizontally aligned ZnO microrod/*p*-GaN heterojunction LED, which is actually composed of line pattern with yellow–green emissions observed at forward bias (Figure 4d, insert). The enlarged optical images for the vertically and horizontally aligned ZnO microrods/*p*-GaN LEDs at forward bias is shown in Figure S16, which illustrates the EL emission pattern and color transformation. Parallel threadiness EL emission patterns with the same orientation of the horizontally aligned ZnO microrods/*P*-GaN heterojunction LED could be obtained (Figures S16b, 17). The observed color change from UV–blue to yellow–green accompanied with red emission can be due to the modification of the interface between ZnO and GaN. The lateral view EL image of the vertically aligned ZnO microrods/*p*-GaN heterojunction LED showed only UV–blue emission color (Figure S18), which is consitent with the top-view image.

Figure 5 shows the schematic energy band diagrams and carrier transitions of the vertically and horizontally aligned ZnO microrods/*P*-GaN heterojunctions. The piezoelectric effect and energy band bending are illustrated to explain the possible mechanism of carrier transport characteristics when ZnO microrods are freely standing or bent for vertically and horizontally aligned ZnO microrods/*P*-GaN heterojunction LEDs. Electrons possess higher mobility in ZnO than holes in *p*-GaN. The electrons have a high probability of transit from the side of ZnO to *p*-GaN through the interface, which resulted in the recombination where ZnO microrods are located. Considering the EL emission differences of the vertically and horizontally aligned ZnO microrods/*p*-GaN LEDs, the changes in interface states during the combing process should be considered. Stress-induced photoluminescence in ZnO structure can be used as a self-reporting sensor. During the transformation from the vertically to the horizontally aligned ZnO microrods, the strain-induced bandgap reduction and the generation of interface states may reduce UV–blue recombination radiation accompained by a redshift and an increased yellow–green emission band.[36–38] The EL spectra of the horizontally aligned ZnO microrods/*p*-GaN heterostructure LED showed a broad emission band that dominated the visible region from 500 nm to 700 nm and accompanied by weak UV–blue emission peaks that are governed by the electronic properties of ZnO and GaN layers and the interface properties. A possible explanation of the decrease in the injection current for the horizontally aligned ZnO microrods/*p*-GaN heterojunction LED is the carrier depletion effect, which is due to the generation of interface states and the building of a charge depletion zone by bending the ZnO microrods during the combing process.[35] When the ZnO microrods are bent by an external force, the piezoelectric effect-induced potential on the interface potential barrier causes the increase in the effective

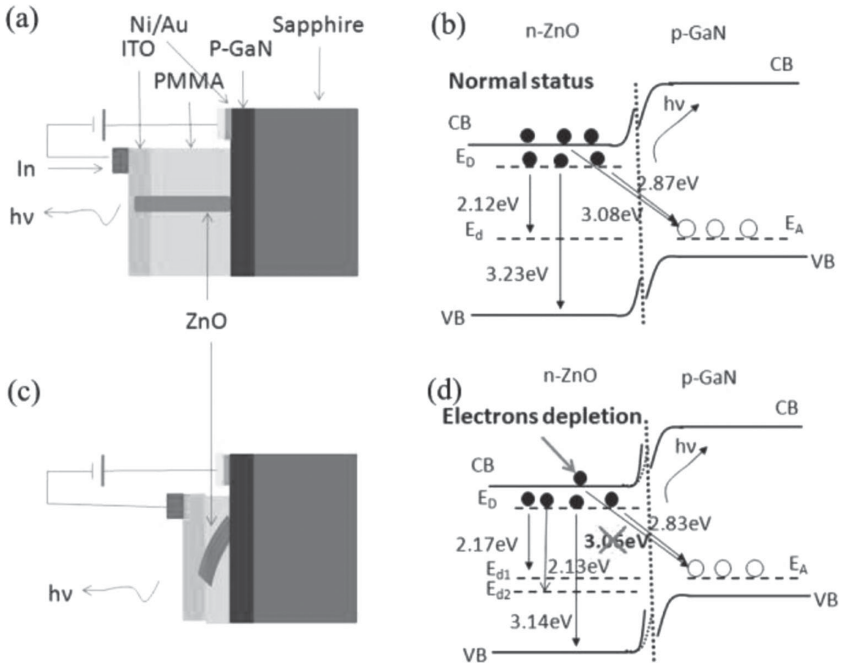

Figure 5. (a–d) Schematic diagrams illustrating the piezoelectric effect and energy band bending to explain the possible mechanisms of carrier transport characteristics when ZnO microrods are freely standing or bent for vertically or horizontally aligned ZnO microrods/*P*-GaN heterojunction LEDs. VB, E_D, $E_{d1,2}$, E_A and CB are valance band minimum, shallow donor level, deep defects related energy levels, acceptor level and conduction band maximum, respectively.

potential barrier, and influences the recombination properties of the LED.[39] Piezoelectric effect can influence the electronic transport characteristics of ZnO microrods, and the interface states between ZnO and *p*-GaN layers in heterojunction LED play an important role in radiative recombination. For the horizontally aligned ZnO microrods, the electron depletion at the interface states increases the threshold and decreases the effective radiative recombination from the conductive band in ZnO to the acceptor level in *p*-GaN (Figure 5d), which is in accordance with the EL spectrum for the horizontally aligned ZnO microrods/*p*-GaN heterojunction LED [radiative recombination at 3.08 eV (~402 nm) was not observed in the EL spectrum]. In addition, the effects of the ZnO material itself, or interfaces between ZnO microrod and *p*-GaN, or the ITO electrode contact issues with the microrods (especially for the horizontally aligned ones) on the uniformity of light emission should be considered. Piezoelectric effect can influence the electronic transport characteristics in ZnO microrods, and the interface states between ZnO and *p*-GaN layers in heterojunction LED have a significant effect on the efficient radiative recombination. The results indicate that the ZnO can be a suitable waveguide material in the UV and visible spectral range. The obtained optical images show considerable variation in output intensity. However, the obtained EL emission patterns (from spot to line shaped) can be captured for the vertically and horizontally aligned ZnO microrods/*p*-GaN heterojunction LEDs. Moreover, the emission color from UV–blue to yellow–green can be tuned from the vertically to the horizontally aligned ZnO microrods/*p*-GaN heterojunction LEDs, which further demonstrate that a kind of piezo-phototronic sensor can be built for pressure transduction. To understand the effects of piezoelectricity on the carrier-transport properties of the ZnO microrods, the *I–V* characteristics of the ZnO microrod (Figure S19) were measured with free-standing (free contact within electrode) or bent (with external force) modes. As shown in Figure S18a, by gradually bending the ZnO microrod, nonlinear *I–V* curves accompanied with lowered injection current were observed, which demonstrated that a barrier was built for blocking the transport of the carrier. When the external force was revoked, the original linear *I–V* characteristic was observed. When the electrode of the bent side for the ZnO microrod is replaced by Au metal, a similar result (piezoelectric properties of the ZnO under bending state produce a barrier layer that result in larger threshold voltage) was observed (Figure S19b).

3. Conclusion

Large-scale horizontally aligned ZnO microrod arrays with periodic alignment and controlled orientation were fabricated via the combing technology. The chip in piezo-phototronic devices such as LEDs can be built based on the horizontally aligned ZnO microrods on the *p*-GaN layer, the transformation from spot to line shaped EL emission patterns could be captured. The EL emission properties of the material were modified because of the piezoelectric effect-induced interface barrier and the generation of interficial state energy levels during the combing procedure, which resulted in the decrease of the UV–blue emission accompanied with a redshift, disappearence of the 3.08 eV EL transition and the increase of the deep energy level related yellow–green emission. Based on these observations the EL emission patterns, colors could be tuned based on ZnO microrods/*p*-GaN heterojunction LEDs, which meant the built photo-emission device could be used as piezoelectric sensors in the applications of pressure transduction. More importantly, our experiments opened a possible way to build large-scale micro- or nanostructured LEDs, as well as other photoelectronic units for the integration of chip devices in laboratories. Therefore, the proposed combing method can be applied to transform aligned distribution from vertical to horizonal orientation for micro- or nanostructures with any designed patterns and materials for building chip in devices.

4. Experimental Section

Synthesizing Vertically Aligned ZnO Microrod Arrays: First, a thin layer of PMMA (MicroChem Corp., 950 K, 3 wt% in

chlorobenzene) with a thickness of ~100 nm was spin-coated on a *p*-GaN layer, which was used as the template, at a rotation speed of 3000 rpm for 40 s. The *p*-GaN/sapphire substrate was cleaned using organic solvents and rinsed with deionized water to remove contaminations. Before being loaded into the electron beam lithography (EBL) direct write chamber, the PMMA layer was baked on a hot plate at 180 °C for 2 min to flatten the film, remove the residual solvent, and enhance the adhesion between PMMA and substrate. The film was then cooled down to room temperature. The accelerating voltage, spot size, and current of the electron beam were 20 kV, 10 nm, and 0.279 nA, respectively. The write field was 100 μm × 100 μm. After exposure, the PMMA films were developed with 1:3 methyl isobutyl ketone:isopropanol (MIBK:IPA) at 20 °C for 40 s, then rinsed in pure IPA for 30 s, and finally dried with nitrogen gas. The hydrothermal method was then performed to explore the growth of vertically aligned ZnO microrods on the exposed *p*-GaN layer by using $Zn(CH_3COO)_2{\cdot}2H_2O$ and $C_6H_{12}N_4$ as reactant sources. The reaction solution was adjusted to an identical concentration (0.02 mol/L), and the surface of the *p*-GaN layer was loaded toward the bottom of the reaction kettle. The reaction kettle was placed in an oven and maintained at 95 °C for 6 h. The obtained samples were rinsed with deionized water and dried in the oven.

Preparing Combing Structure: A layer of photoresist (AZ701) with a thickness of around 1 μm was spin-coated on a quartz glass wafer at a rotation speed of 2000 rpm. The photoresist was pre-baked at 95 °C for 5 min, and the photoligraphy was performed with vacuum and hard contact mode, with constant UV exposure time of 45s. The development procedure were carried out with MIF300 for 45s. The combing structure was then dried with nitrogen gas and post-baked at 120 °C for 5 min.

Preparing Horizontally Aligned ZnO Microrod Arrays: The horizontally aligned ZnO microrod arrays were fabricated using EVG 620 photolithography machine, which is equipped with a nano-imprinting function. The synthesized vertically aligned ZnO microrod arrays on the *p*-GaN/sapphire substrate was first loaded into the sample holder.The combing structure/quartz glass was loaded in as a mask, and both were then aligned using markers with a positive alignment accuracy of 0.8 μm. The approaching distance was adjusted to confine the vertically aligned ZnO microrod arrays in the combing structure such that the top of the ZnO microrod arrays completely touches the combing structure. A shift of a few micrometer of x-axis, y-axis, or θ-rotation in a plane for the sample holder could result in certain angle tilting for the vertically aligned ZnO microrods. Continued force was then applied top-down, and the horizontally aligned ZnO microrod arrays on the *p*-GaN/sapphire substrate was obtained.

Apparatus Applied: The EBL pattern for PMMA was obtained using the Raith150 TWO equipment. The combing procedure was performed using EVG 620 photolithography machine, which is equipped with a nano-imprinting function. The morphology of the sample was investigated via field emission scanning electron microscopy (FESEM) (Hitachi S-4800 microscope). The crystal structure of the sample was studied usinga Bruker D8GADDS X-ray diffractometer with Cu-Kα rradiation. Photoluminescence (PL) measurement was performed using a JY-630 micro-Raman spectrometer with 325 nm line of He–Cd laser as the excitation source. The EL spectra were performed by a Hitachi F4600 spectrometer, and a continuous-current power source was used to excite the LEDs. Current versus voltage (*I*–*V*) measurement was performed by a Hall measurement system (Lakeshore 7400). Note that all the measurements were performed at room temperature.

Supporting Information

Supporting Information is available from the Wiley Online Library or from the author.

Acknowledgements

This work is supported by the National Natural Science Foundation of China under Grant Nos. (51202154, 51205268), the Natural Science Foundation of Jiangsu Province under Grant Nos. (BK20131169, BK2012190), National 863 Key Project under Grant No. 2012AA040503, the Science Technology development program of Suzhou city under Grant No. ZXY2012011, the Nano-technology for special project of Suzhou city under Grant No. ZXG2013038, and the SRF for ROCS, SEM.

[1] A. Tsukazaki, A. Ohtomo, T. Onuma, M. Ohtani, T. Makino, M. Sumiya, M. Kawasaki, *Nat. Mater.* **2004**, *4*, 42.
[2] D. Wiersma, *Nature* **2000**, *406*, 132.
[3] S. Chu, G. Wang, W. Zhou, Y. Lin, L. Chernyak, J. Zhao, J. Liu, *Nat. Nanotechnol.* **2011**, *6*, 506.
[4] M. A. Versteegh, D. Vanmaekelbergh, J. I. Dijkhuis, *Phys. Rev. Lett.* **2012**, *108*, 157402.
[5] X. Wang, X. Wang, J. Zhou, J. Song, J. Liu, N. Xu, Z. L. Wang, *Nano. Lett.* **2006**, *6*, 2768.
[6] M. Tsaroucha, Y. Aksu, E. Irran, M. Driess, *Chem. Mater.* **2011**, *23*, 2428.
[7] P. Atanasova, D. Rothenstein, J. J. Schneider, R. C. Hoffmann, S. Dilfer, S. Eiben, J. Bill, *Adv. Mater.* **2011**, *23*, 4918.
[8] C. Soci, A. Zhang, B. Xiang, S. A. Dayeh, D. P. R. Aplin, J. Park, D. Wang, *Nano. Lett.* **2007**, *7*, 1003.
[9] Y. Jin, J. Wang, B. Sun, J. C. Blakesley, N. C. Greenham, *Nano. Lett.* **2008**, *8*, 1649.
[10] Z. Zhan, L. Zheng, Y. Pan, G. Sun, L. Li, *J. Mater. Chem.* **2012**, *22*, 2589.
[11] Z. L. Wang, J. Song, *Science* **2006**, *312*, 242.
[12] R. Yang, Y. Qin, L. Dai, Z. L. Wang, *Nat. Nanotechnol.* **2008**, *4*, 34.
[13] F. R. Fan, Z. Q. Tian, L. Z. Wang, *Nano. Energ.* **2012**, *1*, 328.
[14] J. I. Sohn, S. N. Cha, B. G. Song, S. Lee, S. M. Kim, J. Ku, K. Kim, *Energ. Environ. Sci* **2013**, *6*, 97.
[15] M. H. Huang, S. Mao, H. Feick, H. Yan, Y. Wu, H. Kind, P. Yang, *Science* **2001**, *292*, 1897.
[16] X. Wang, J. Zhou, J. Song, J. Liu, N. Xu, Z. L. Wang, *Nano Letters* **2006**, *6*, 2768.
[17] Z. L. Wang, J. H. Song, *Science* **2006**, *312*, 242.
[18] H. Jin, J. Zhou, X. He, W. Wang, H. Guo, S. Dong, D. Wang, Y. Xu, J. Geng, J. K. Luo, W. I. Milne. *Sci. Rep.* **2013**, *3*, 2140.
[19] R. H. Baughman, A. A. Zakhidov, W. A. de Heer, *Science* **2002**, *297*, 787.
[20] T. Yamada, Y. Hayamizu, Y. Yamamoto, Y. Yomogida, A. Izadi-Najafabadi, D. N. Futaba, K. A. Hata, *Nat. Nanotechnol.* **2011**, *6*, 296.
[21] S. Chen, J. G. Bomer, W. G. van der Wiel, E. T. Carlen, A. van den Berg, *ACS Nano* **2009**, *3*, 3485.

[22] M. Lee, Y. Jeon, T. Moon, S. Kim, *ACS Nano* **2011**, *5*, 2629.
[23] R. A. Minamisawa, M. J. Süess, R. Spolenak, *Nat. Commun.* **2012**, *3*, 1096.
[24] F. Liu, H. Gan, D. M. Tang, Y. Cao, X. Mo, J. Chen, Y. Bando, *Small* **2013**, *10*, 685
[25] R. Chen, T. T. D. Tran, K. W. Ng, W. S. Ko, L. C. Chuang, F. G. Sedgwick, C. Chang-Hasnain, *Nat. Photonics* **2011**, *5*, 170.
[26] K. W. Ng, T. T. D. Tran, W. S. Ko, R. Chen, F. Lu, C. Chang-Hasnain, *Nano. Lett.* **2013**, *13*, 5931.
[27] Y. Qin, R. Yang, Z. L. Wang, *J. Phys. Chem. C* **2008**, *112*, 18734.
[28] S. Xu, Y. Ding, Y. Wei, H. Fang, Y. Shen, A. K. Sood, Z. L. Wang, *J. Am. Chem. Soc.* **2009**, *131*, 6670.
[29] Z. Jin, H. Chu, J. Wang, J. Hong, W. Tan, Y. Li, *Nano. Lett.* **2007**, *7*, 2073.
[30] G. D. Yuan, W. J. Zhang, J. S. Jie, X. Fan, J. A. Zapien, Y. H. Leung, L. B. Luo, P. F. Wang, C. S. Lee, S. T. Lee, *Nano Lett.* **2008**, *8*, 2591.
[31] J. Goldberger, D. J. Sirbuly, M. Law, P. Yang. *J. Phys. Chem. B* **2005**, *109*, 9.
[32] C. H. Chen, S. J. Chang, S. P. Chang, M. J. Li, I. C. Chen, T. J. Hsueh, C. L. Hsu, *Appl. Phys. Lett.* **2009**, *95*, 223101.
[33] T. Nobis, E. M. Kaidashev, A. Rahm, M. Lorenz, M. Grundmann, *Phys. Rev. Lett.* **2004**, *93*, 103903.
[34] T. Nobis, M. Grundmann, *Phys. Rev. A* **2005**, *72*, 063806.
[35] C. Czekalla, C. Sturm, R. Schmidt-Grund, B. Cao, M. Lorenz, M. Grundmann, *Appl. Phys. Lett.* **2008**. *92*, 241102.
[36] B. Wei, K. Zheng, Y. Ji, Y. Zhang, Z. Zhang, X. Han, *Nano. Lett.* **2012**, *12*, 4595.
[37] X. Jin, M. Götz, S. Wille, Y. K. Mishra, R. Adelung, C. Zollfrank, *Adv. Mater.* **2013**. *25*, 1342.
[38] X. Wang, X. Wang, J. Zhou, J. Song, J. Liu, N. Xu, Z. L. Wang, *Nano. Lett.* **2006**, *6*, 2768.
[39] S. S. Kwon, W. K. Hong, G. Jo, J. Maeng, T. W. Kim, S. Song, T. Lee, *Adv. Mater.* **2008**, *20*, 4557.

Received: July 21, 2014
Published online: September 15, 2014